AAS 24-143

GUIDANCE AND CONTROL FOR LASER-BASED NON-COOPERATIVE TARGET DETUMBLING

Corey L. Marcus*, Andres Dono Perez†, and Renato Zanetti‡

Large pieces of orbital debris form a significant risk of fragmentation in case of collision. Such fragmentation would greatly increase the number of trackable and untrackable debris on orbit. This makes them attractive targets for future rendezvous and disposal missions. However, these non-cooperative targets tend to be tumbling and rendezvous with them is a dangerous prospect. To avoid this danger, contactless detumbling through laser ablation has been proposed prior to rendezvous. Existing proposals for contactless laser-based detumbling have yet to include an in-depth study of the problem's guidance, navigation, and control requirements. In this work we develop an attitude and relative motion control scheme for a chaser satellite detumbling a non-cooperative target via laser. We show that detumbling can be achieved with reasonable time and dV budgets. With Monte Carlo methods we explore the impact of laser force on the detumbling operation and reveal some non-intuitive relationships.

INTRODUCTION

Orbital debris is a fast growing problem. There are approximately one million objects in Earth orbit greater than one centimeter in diameter. Of these 36,500 are larger than 10 centimeters and can be tracked via earth observations.[1] As human space presence increases, these numbers are likely to grow. Some authors predict exponential growth of the number of debris.[2] This represents a huge risk to current and future space activities due to the risk of collision. An infamous worst case scenario noted by Kessler and Cour-Palais would result in large orbital bands becoming unusable due to cascading collisions.[3]

Many strategies have been proposed to prevent future spacecraft from contributing to this problem. They include deployable hardware such as conductive tape[4] and reflective balloons[5] which are designed to decrease the time to spacecraft reentry. Procedural changes are also proposed which simply require the spacecraft to maneuver to a graveyard orbit where it either will not interfere with other spacecraft or is expected to reenter within a reasonable time frame. Today, almost all space missions have some disposal plan. The space agencies of many nations have agreed to guidelines developed by the Inter-Agency Space Debris Coordination Committee which require disposal within 25 years of mission end, among other things.[6]

These strategies do not address the large number of debris which are already on orbit and so a variety of debris management systems have been proposed. Sweepers are spacecraft with a large shield that physically impacts small debris, slowing them enough to reenter.[7] Rapid response rockets contain a payload of dust and are launched when an imminent collision between debris and another object is detected. The payload is deployed into a cloud on a ballistic trajectory that the

*Graduate Student, Aerospace Engineering, The University of Texas at Austin
†Flight Dynamics Team Lead, Axient/NASA Ames Research Center, Moffett Field, California
‡AAS Fellow, Associate Professor, Aerospace Engineering, The University of Texas at Austin

debris will pass through. If performed early enough, this perturbation on the debris' orbit can prevent collision.[8] A variety of schemes involving lasers have been proposed.[9–11] The lasers might be located on the ground or orbital platforms. Selected pieces of debris are targeted and have their surface ablated, which generates thrust. This thrust might be used to deorbit the targeted debris or alter its orbit to prevent a collision. Another method involves orbital tugs. An active spacecraft might rendezvous with the debris and then use its own thrusters to alter the target's orbit or deorbit outright.[12]

Large pieces of debris present attractive targets for remediation. In case of collisions, these objects could fragment into thousands or tens of thousands of new pieces of debris. This has happened several times in the past, most notably the collision between Iridium 33 and Kosmos 2251, which generated 1,632 pieces of new debris.[13]

Most proposals for dealing with large debris are orbital tugs and thus require rendezvous. This is a dangerous prospect as the defunct pieces of debris tend to be tumbling. Some techniques have been proposed to rendezvous with these tumbling targets but have not been demonstrated with real spacecraft.[14] One recent flight test successfully captured an object with a net.[15] The same mission also demonstrated a capture strategy based on harpoon. Regardless of the specifics, rendezvous with these tumbling targets is a dangerous operation. Inadvertent collisions could easily incapacitate the orbital tug and result in two pieces of large debris where previously there was one.

Laser ablation is proposed as a contactless method for deorbiting debris and thus avoids many of the perils associated with rendezvous. Mission concepts such as L'ADROIT propose an orbital laser platform which may target large pieces of debris for perturbation and small pieces for reentry.[10] The principal problem is that ablation is low thrust compared to a traditional liquid propellant system. Vacuum chamber experiments have shown ablation thrusts on the order of millinewtons could be created by a $100\,\mathrm{W}$ laser $100\,\mathrm{m}$ from the target with a $10\,\mathrm{cm}$ optical diameter.[16] Real world scenarios might have infrequent targeting windows and performance losses due to imperfect laser operation. In these scenarios, the effective continuous thrust might be several orders of magnitude lower.

Some authors have proposed using ablation to regulate a target's angular rate to zero; a process referred to as detumbling. In this work we study guidance and control strategies for this concept. Our proposed remediation vehicle will be equipped with an onboard laser and a suite of robotic manipulators which enable rendezvous with a targeted piece of debris. We propose a two-phase methodology for large debris remediation. In the first phase our vehicle will approach and use its onboard laser to detumble the target. At this point we rendezvous with the target and the second phase begins. Our vehicle uses its own thrusters to alter the orbit of both vehicles or deposits a propulsion module that accomplishes the same task after the remediation vehicle has departed. For this study we've designed an attitude and relative motion control system for the target detumbling operation in phase one. We will study how variations in laser ablative force affects remediation vehicle fuel consumption and detumble time. Future work will study a more complete mission concept which includes the actual rendezvous operation after detumbling is complete.

RELATED WORK

Rendezvous with tumbling targets is a complex guidance, navigation, and control problem. Michael et al. find a solution to the guidance sub-problem with direct optimization methods.[17] However, they require a priori knowledge of the relative spacecraft state and target inertia tensor. In this work, we

assume knowledge of the true target angular rate. In practical applications some estimation scheme would be required such as the one developed by Almeida et al using monocular cameras.[18] Albee et al provide an end-to-end solution for rendezvous with tumbling targets and demonstrate its efficacy with NASA's Astrobee on the International Space Station.[14] Some mission designers may view rendezvous with tumbling targets as an unacceptable risk. The risk could be greatly reduced and these maneuvers could be eliminated if the target was detumbled prior to rendezvous.

Laser-based debris remediation is a frequently studied concept. The photon pressure is not significant enough to meaningfully affect most pieces of debris so the general concept of operations typically calls for ablation of the target surface. Thrust is produced as material is vaporized. Generally, the authors call for lasers that are either ground-based or space-based. One ground based-architecture calls for lasers which provide high precision range measurements to targets previously acquired via radar.[19] These high precision measurements can refine the target's estimated orbit and reduce false alarms in conjunction analysis. The author proposes that the same lasers may also be used to nudge targets and reduce the risk of conjunction. One notable space-based laser remediation concept is known as Laser Ablative Debris Removal by Orbital Impulse Transfer (L'ADROIT).[10] L'ADROIT proposes using a 20-40 kW laser to re-enter small pieces of debris and perturb larger ones. Both propositions first acquire a target is with a wide field-of-view sensor such as radar or a camera. Next, laser pulses are used in a ranging mode to obtain a precise target orbit determination. Finally, this precise orbit determination is used to target the laser for remediation purposes. Neither work contains an in-depth design and validation of the estimation and control algorithms these processes would require.

Several authors have studied laser-based satellite detumbling. One study develops a simple controller which aims to impart the maximum control torque opposite the direction of angular velocity.[20] Their implementation contains a navigation scheme in the loop and a combination of laser-range and optical measurements are used to estimate angular velocity. They show that since the force from ablation is always orthogonal to the targeted surface, some axes of rotation are uncontrollable for cylindrical objects. Another implementation contains a more complex proportional-derivative control scheme for box-shaped targets.[21] With this scheme they can regulate target attitude in addition to angular rate. They are unable to prove controllability or stability but suggest both might be true through Monte Carlo. Neither control scheme addresses the problem of relative motion control.

Lasers are not the only contactless method for detumbling, others have explored electrostatic forces.[22] However, the torques induced by these methods are only significant at ranges on the order of 10 meters. This can be contrasted with effective laser range on the order of hundreds of meters to hundreds of kilometers depending on the laser size and quality. Approaching a non-cooperative and tumbling target close enough for electrostatic detumbling may be too risky for some missions.

METHODOLOGY

We have designed a guidance and control scheme for a chaser vehicle using a laser to autonomously detumble a non-cooperative target. Our system contains three primary software modules:

1. Laser Controller: A feedback controller for the desired irradiation point on the target's surface

2. Attitude Controller: A feedback controller to regulate the chaser's attitude and angular rate

3. Relative Motion Controller: An open-loop guidance law to maintain formation flight between the chaser and target

These modules are outlined in Figure 1. The kinematic and dynamic plant models for the chaser and target are represented with red blocks while each software module is represented with black blocks. Each plant contains a kinematics and dynamics model for the vehicle's position, velocity, attitude, and angular rate. Position and velocity are propagated with a two-body gravity model. Attitude and angular rate use a rigid body model. There is a coupling between the chaser and target plant models as the chaser's laser direction d_{laser} controls the irradiation point on the target from which an ablative force emanates.

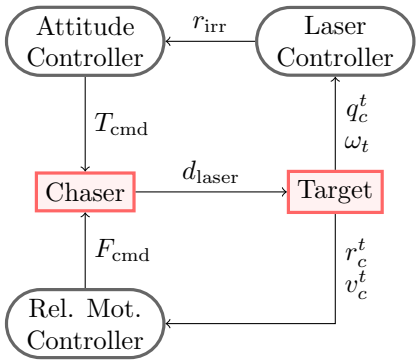

Figure 1 A high level overview of our control system. The target's attitude and angular rate are supplied to the Laser Controller. The Laser Controller provides an irradiation point on the target body to the Attitude Controller. The Attitude Controller finds torque commands such that the chaser's laser impacts the desired irradiation point. The targets position and velocity are supplied to the Relative Motion Controller which finds chaser thrust commands to maintain formation flight.

The laser controller takes as inputs the quaternion describing the relative attitude from chaser to target frame q_c^t and the target's angular rate ω_t. It outputs the desired irradiation point on the target body r_{irr}. The attitude controller takes in r_{irr} and outputs torque commands T_{cmd} for the chaser. The relative motion controller takes in the relative position r_c^t and velocity v_c^t and outputs force commands F_{cmd} for the chaser's thrusters.

Laser Control

Our laser control system is a modified version of the one described by Sakai et al.[21] It contains a feedback controller which regulates the target's angular rate by choosing a targeted irradiation point r_{irr}. We aim only to detumble the target and do not control attitude.

We assume our chaser has the ability to tightly focus its laser on the target's surface. Irradiation in this manner ablates small amounts of surface material. The ablated material is largely vaporized and off-gassed omnidirectionally in a process which is mostly independent of irradiation direction. This process is illustrated in figure 2. The ablative off-gassing induces a force upon the target surface which is several orders of magnitude larger than photon pressure. Exactly modeling this thrust an

active area of research. We use a simplified model inspired by[20,21,23] where the force is simply orthogonal to the target surface at the irradiation point as shown in Equation (1) where f_{laser} is the force magnitude and $\hat{n}$ is the surface normal at the irradiation point. We assume f_{laser} is a constant value. In reality it will vary based on factors such as but not limited to the laser's range, duty cycle, angle of incidence, and target material.

$$F_{\text{laser}} = -f_{\text{laser}}\hat{n} \tag{1}$$

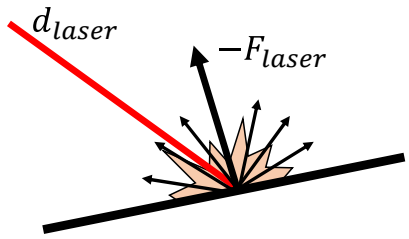

Figure 2 A diagram of the laser ablation model. The laser arrives along d_{laser} and begins to ablate material upon the target surface. This material is off-gassed omnidirectionally such that the net force upon the surface F_{laser} is orthogonal to it.

The controller chooses a reference torque by assuming arbitrary control torques are available. Then an irradiation point is chosen on one of the visible faces which minimizes the difference between the reference torque and actual applied torque. The reference torque is simple in nature and opposes the target's angular rate with respect to an inertial frame ω_t^i.

$$T_{\text{ref}} = -k_{p,\text{laser}}\omega_t^i \tag{2}$$

Here, $k_{p,\text{laser}}$ is a proportional gain. Overshoot and steady-state error are not a concern since angular rate alone is a first-order system. This means derivative and integral control terms are not necessary.

Our target is modeled as a box shaped satellite as shown in Figure 3. No more than three and no less than one face will be visible to our chaser at any time. Our laser control module aims to choose an irradiation point on the target r_{irr} to minimize the difference between T_{ref} and the applied torque.

We begin with the location of the laser expressed in the target body frame r_{laser} and determine a set of N_{viz} visible faces. Each corresponds to a surface normal $\hat{n}_i$, orthogonal distance from the origin d_i, length, and width. Our target body frame is defined such that each $\hat{n}_i$ is parallel or anti-parallel to one of the standard x, y, or z basis vectors. This setup is diagrammed in Figure 4.

We approximate the angle θ_i between each visible face and the laser vector as

$$\theta = \cos^{-1}\left(\frac{\hat{n}_i^T r_{\text{laser}}}{||r_{\text{laser}}||}\right). \tag{3}$$

When θ is high the irradiated area on the target surface will grow and laser fluence will therefore drop. Ablation occurs only above a certain fluence threshold. When the θ grows there will likely come a time when the fluence on target drops below this threshold and the applied force sharply

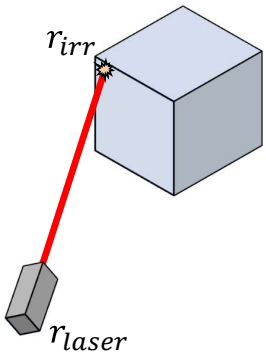

Figure 3 A diagram of the visible target surfaces. The laser is located at r_{laser} and the point r_{irr} must be chosen from the visible surfaces.

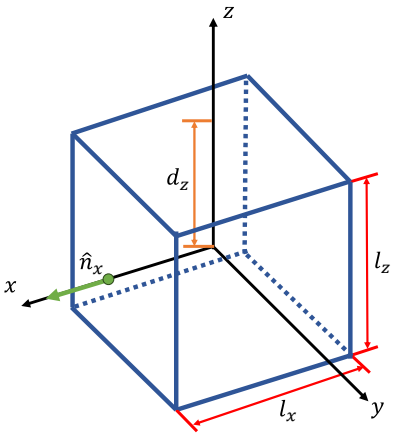

Figure 4 The target's physical model and body coordinate frame. The body frame's origin is located at the target's geometric center. The orthogonal distance between each body face and the origin is d_i, an example is labeled for the z axis. Each body face has an associated surface normal which is parallel or anti-parallel to one of the frame's basis vectors, an example is highlighted for the x axis. Each principal axis also has an associated length l_i. l_x and l_z are labeled as an example.

drops by several orders of magnitude. Therefore, we do not consider targeting faces in which $\theta > 75°$. The ablative force upon the target for each visible face is found as

$$F_{\text{laser}} = -f_{\text{laser}}\hat{n}_i. \tag{4}$$

The torque produced by Equation (4) is

$$T_i = \left(I_3 - \hat{n}_i\hat{n}_i^T\right) C \tag{5}$$

where $C \in \mathbb{R}^3$ is a vector to be solved for. The matrix $\left(I_3 - \hat{n}_i\hat{n}_i^T\right)$ is not full rank which indicates incomplete control authority. This implies that under certain conditions the target's angular rate will be uncontrollable. The previous work of Sakai et al.[21] showed that such scenarios are likely to be transitory due to the relative motion of the two spacecraft.

We aim to minimize the cost J.

$$J = (T_{\text{ref}} - T_i)^T (T_{\text{ref}} - T_i) \tag{6}$$

After substituting Equation (5), differentiating with respect to C, and simplifying we arrive at the following condition.

$$\left(I_3 - \hat{n}_i \hat{n}_i^T\right) T_{\text{ref}} = \left(I_3 - \hat{n}_i \hat{n}_i^T\right) C \tag{7}$$

From this it is easy to see that choosing

$$T_i = \left(I_3 - \hat{n}_i \hat{n}_i^T\right) T_{\text{ref}} \tag{8}$$

satisfies the first order necessary conditions for optimality. However; we are constrained by the finite dimensions of the target surface and T_i may not be physically realizable. An irradiation point can be broken into its components that are orthogonal and in-plane of the target surface.

$$r_{\text{irr}} = r_{\text{irr}}^{\perp} + r_{\text{irr}}^{\square} \tag{9}$$

The orthogonal component is completely constrained by the target's geometry and is found as

$$r_{\text{irr}}^{\perp} = d_i \hat{n}_i. \tag{10}$$

The in plane component may be described as

$$r_{\text{irr}}^{\square} = \left(I_3 - \hat{n}_i \hat{n}_i^T\right) b \tag{11}$$

where $b \in \mathbb{R}^3$ some vector to be solved for. We perform an eigen decomposition on the matrix $\left(I_3 - \hat{n}_i \hat{n}_i^T\right)$ to find

$$\left(I_3 - \hat{n}_i \hat{n}_i^T\right) = \begin{bmatrix} \hat{n} & e_1 & e_2 \end{bmatrix} \begin{bmatrix} 0 & 0 & 0 \\ 0 & 1 & 0 \\ 0 & 0 & 1 \end{bmatrix} \begin{bmatrix} \hat{n} & e_1 & e_2 \end{bmatrix}^{-1}. \tag{12}$$

Noting that the vectors $\hat{n}$, e_1, and e_2 form an orthonormal basis

$$r_{\text{irr}}^{\square} = \chi e_1 + \gamma e_2. \tag{13}$$

We will solve for scalars χ and γ. Using $T_i = r_{\text{irr}} \times F_{\text{laser}}$, Equations (4), and (8) we write

$$\left(I_3 - \hat{n}_i \hat{n}_i^T\right) T_{\text{ref}} = T_i \tag{14}$$

$$\left(I_3 - \hat{n}_i \hat{n}_i^T\right) T_{\text{ref}} = \left(r_{\text{irr}}^{\perp} + r_{\text{irr}}^{\square}\right) \times -f_{\text{laser}} \hat{n}_i \tag{15}$$

$$\left(I_3 - \hat{n}_i \hat{n}_i^T\right) T_{\text{ref}} = (d_i \hat{n}_i + \chi e_1 + \gamma e_2) \times -f_{\text{laser}} \hat{n}_i \tag{16}$$

$$\left(I_3 - \hat{n}_i \hat{n}_i^T\right) T_{\text{ref}} = \chi f_{\text{laser}} e_2 - \gamma f_{\text{laser}} e_1 \tag{17}$$

$$\begin{bmatrix} \mathbf{0}_{3\times 1} & e_1 & e_2 \end{bmatrix} \begin{bmatrix} \hat{n} & e_1 & e_2 \end{bmatrix}^{-1} T_{\text{ref}} = f_{\text{laser}} \begin{bmatrix} \mathbf{0}_{3\times 1} & -e_1 & e_2 \end{bmatrix} \begin{bmatrix} 0 \\ \gamma \\ \chi \end{bmatrix} \tag{18}$$

$$\frac{1}{f_{\text{laser}}} \begin{bmatrix} \mathbf{0}_{1\times 3} \\ -e_1^T \\ e_2^T \end{bmatrix} \begin{bmatrix} \mathbf{0}_{3\times 1} & e_1 & e_2 \end{bmatrix} \begin{bmatrix} \hat{n} & e_1 & e_2 \end{bmatrix}^{-1} T_{\text{ref}} = \begin{bmatrix} \mathbf{0}_{1\times 3} \\ -e_1^T \\ e_2^T \end{bmatrix} \begin{bmatrix} \mathbf{0}_{3\times 1} & -e_1 & e_2 \end{bmatrix} \begin{bmatrix} 0 \\ \gamma \\ \chi \end{bmatrix} \tag{19}$$

$$\frac{1}{f_{\text{laser}}} \begin{bmatrix} 0 & 0 & 0 \\ 0 & -1 & 0 \\ 0 & 0 & 1 \end{bmatrix} \begin{bmatrix} \hat{n} & e_1 & e_2 \end{bmatrix}^{-1} T_{\text{ref}} = \begin{bmatrix} 0 \\ \gamma \\ \chi \end{bmatrix} \tag{20}$$

There is one more constraint to handle, the face length l and width w. We require r_{irr} to be on the surface and an additional offset distance away from any edges. This offset is heuristically sized to avoid irradiating an edge or incorrect face resulting from pointing inaccuracies. We saturate our solutions for γ and χ to meet these conditions.

We find r_{irr} for each visible face and target the one that minimizes J without increasing the target's angular momentum.

Attitude Control

The attitude control module ensures the laser accurately targets r_{irr}. The targeted point is transformed into the chaser body frame used to form a reference laser direction $d_{\text{laser, ref}}$. The module compares this reference direction with the true laser direction d_{laser}. This setup is highlighted in Figure 5.

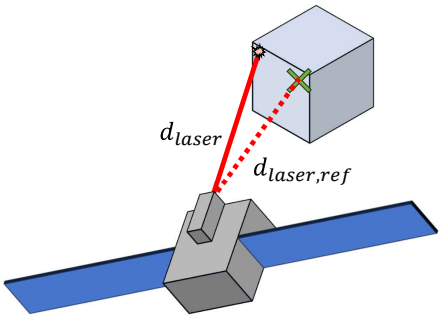

Figure 5 A diagram of the attitude control error. The laser is pointed along d_{laser} while its desired direction is $d_{\text{laser, ref}}$.

Our goal is to produce body torques which will steer d_{laser} such that it will be aligned with the reference. We assume there is no constraint on the direction of our chaser's body torque which is produced by actuators such as reaction wheels. These body torques will be generated with a proportional-derivative (PD) feedback controller. This will require an error signal which we generate from the minimum rotation to align d_{laser} with the reference.

The axis of this rotation $\hat{e}$ is found as

$$\hat{e} = d_{\text{laser}} \times d_{\text{laser, ref}}. \tag{21}$$

The angle ϕ_e is

$$\phi_e = \cos^{-1}\left(d_{\text{laser}}^T d_{\text{laser, ref}}\right). \tag{22}$$

Together $\hat{e}$ and ϕ_e form an Euler axis and angle. These are converted to a quaternion whose vector component becomes our error parametrization.

$$q_{e,v} = \sin\left(\frac{\phi_e}{2}\right)\hat{e}. \tag{23}$$

The commanded chaser body torque is produced by the PD controller as

$$T_{\text{body}} = k_p q_{e,v} + k_d \dot{q}_{e,v} \tag{24}$$

Here k_p and k_d are the proportional and derivative gains. These are tuned to provide acceptable overshoot and settling time without requiring unrealistic body torques. $\dot{q}_{e,v}$ is the time derivative of $q_{e,v}$ and is found numerically using Simulink. Future investigations may use knowledge of the target's body-rate to formulate a reference chaser body-rate. This would eliminate the need for numerical differentiation and likely improve control performance.

Relative Motion Control

Relative motion control is an important component of the detumbling program. The two vehicles will tend to separate as laser force is applied to the target. Periodically we find a set of maneuvers which will eliminate any accumulated drift by restoring a nominal relative orbit. Our nominal relative orbit is known as a safety ellipse (SE). The SE is diagrammed in Figure 6. It is a periodic relative trajectory which forms an ellipse in the target's radial, transverse, normal (RTN) coordinate frame. The chaser travels along this ellipse with a period equal to the orbital period. The ellipse's ascending and descending nodes are located along the radial axis. When the chaser crosses the normal-transverse plane its distance from the transverse axis is maximized.

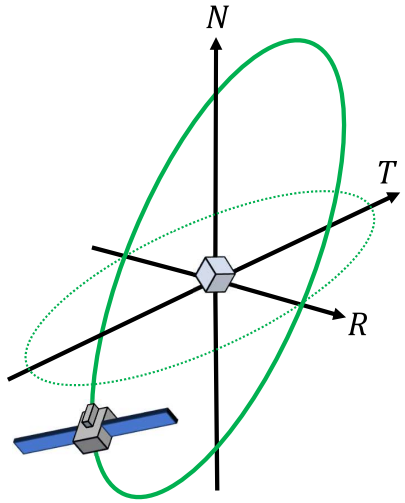

Figure 6 A diagram of the SE. The chaser's motion with respect to the target forms an ellipse in the target's RTN frame. As the chaser crosses the NT plane its distance from the transverse axis is maximized.

The SE has two primary beneficial features. First, it is designed to reduce the chance of collision between the two vehicles by maximizing distance from the transverse axis. Perturbations to either vehicle's orbit could result in a collision. Unlike the transverse direction, perturbations along the normal and radial directions do not affect the orbital period. Any perturbations to the orbital period would result in the ellipse's center drifting along the transverse direction. If the chaser's motion were to directly cross the transverse axis a collision could occur.

The second benefit is that the target is viewed from a variety of angles in an inertial frame. The laser's incomplete control authority means that if the target is not viewed from multiple angles angular momentum aligned with the d_{laser} can not be regulated. In addition, when the target is viewed from multiple angles the force applied to the target more closely averages to zero over the

course of an orbital period. This results in less relative drift between the two vehicles and implies fewer restorative maneuvers will be required. We note that the average relative inertial position of a vehicle in an SE is not zero. Future work will investigate relative motion regimes in which this is the case.

SEs can be specified in terms of the D'Amico[24] relative orbital elements (rOE), which are shown in Equation (25).

$$\delta\alpha = \begin{bmatrix} \delta a \\ \delta\lambda \\ \delta e_x \\ \delta e_i \\ \delta i_x \\ \delta i_y \end{bmatrix} = \begin{bmatrix} (a_c - a_t)/a_t \\ (u_c - u_t) + (\Omega_c - \Omega_t)\cos(i_t) \\ e_c\cos(\omega_c) - e_t\cos(\omega_t) \\ e_c\sin(\omega_c) - e_t\sin(\omega_t) \\ i_c - i_t \\ (\Omega_c - \Omega_t)\sin(i_t) \end{bmatrix} \tag{25}$$

Here, c and t subscripts denote chaser and target, respectively. a, e, i, Ω, and ω are the Keplerian orbital elements. u is the mean argument of latitude

$$u = \omega + M \tag{26}$$

where M is the mean anomaly. SEs are formed when the rOEs meet two criteria. First, $\delta a = 0$. This ensures that each vehicle has the same orbital period and so any relative motion is periodic. Second, the δe vector is parallel or anti-parallel to the δi vector. This ensures that the distance between the chaser and transverse axis is maximized as the chaser crosses the normal-tangential plane.

To generate maneuvers which restore our SE we use the methodology developed by Shuster et al.[25] The authors formulate an analytic solution for a three-impulse maneuver sequence which reconfigures existing SEs over the course of one and a half orbits. We violate some of assumptions as their formulation requires a transfer from SE to another. At the time of maneuver initiation the laser force has degraded the SE and so the initial conditions no longer satisfy the SE constraint. The penalty for this is that our maneuvers may not be fuel optimal. Future investigations will quantify these inefficiencies.

We generate maneuver sequences from an initial set of rOEs $\delta\alpha_0$ to a final set $\delta\alpha_f$ from which we define the difference $\Delta\delta\alpha = \delta\alpha_f - \delta\alpha_0$. We find a possible value for the target's mean argument of latitude at the first maneuver u^* as

$$u^* = \mathrm{atan2}(\Delta\delta\alpha(6), \Delta\delta\alpha(5)). \tag{27}$$

When u^* does not equal the target's current mean argument of latitude u_0 we must coast before a maneuver can be performed. The coast period u_{wait} is found as

$$u_{\text{wait}} = \begin{cases} u^* - u_0 + 3\pi & u^* - u_0 < -2\pi \\ u^* - u_0 + 2\pi & -2\pi \leq u^* - u_0 < \pi \\ u^* - u_0 + \pi & -\pi \leq u^* - u_0 < 0 \\ u^* - u_0 & 0 \leq u^* - u_0 \end{cases} \tag{28}$$

The target's mean argument of latitude at each maneuver is found as

$$u_k = u_0 + u_{\text{wait}} + (k-1)\pi \qquad k = \{1,\, 2,\, 3\}\,. \tag{29}$$

Next we find a direction common to all three maneuvers $\Delta\hat{v}$.

$$\Delta\hat{v} = \frac{\Delta\tilde{v}}{\|\Delta\tilde{v}\|} \tag{30}$$

where $\Delta\tilde{v}$ an intermediate quantity. Each of its three RTN components are solved for separately. First we need

$$\eta = \text{sign}\left(\Delta\delta\alpha(5)\cos(u_1) + \Delta\delta\alpha(6)\sin(u_1)\right) \tag{31}$$

and the target's mean motion

$$n = \sqrt{\frac{\mu}{a_t^3}} \tag{32}$$

where μ is the Earth's standard gravitational parameter.

$$\Delta\tilde{v}_R = \frac{\eta n a_t}{\|\Delta\delta\alpha(5:6)\|}\Delta\delta\alpha(5:6)^T \begin{bmatrix} 0 & -1 \\ 1 & 0 \end{bmatrix} \Delta\delta\alpha(3:4) \tag{33}$$

$$\Delta\tilde{v}_T = \frac{\eta n a_t}{2\,\|\Delta\delta\alpha(5:6)\|}\Delta\delta\alpha(5:6)^T\Delta\delta\alpha(3:4) \tag{34}$$

$$\Delta\tilde{v}_N = \eta n a_t \,\|\Delta\delta\alpha(5:6)\| \tag{35}$$

We now know the locations and directions of each maneuver. Their scale factors β_k are found by solving the following system of equations.

$$\begin{bmatrix} 2\Delta\hat{v}_T & 2\Delta\hat{v}_T & 2\Delta\hat{v}_T \\ -2\Delta\hat{v}_R - 6\pi\Delta\hat{v}_T & -2\Delta\hat{v}_R - 3\pi\Delta\hat{v}_T & -2\Delta\hat{v}_R \\ 1 & -1 & 1 \end{bmatrix} \begin{bmatrix} \beta_1 \\ \beta_2 \\ \beta_3 \end{bmatrix} = Q \tag{36}$$

$$Q = \begin{bmatrix} n a_t \Delta\delta\alpha(1) \\ n a_t \left(\Delta\delta\alpha(2) + \frac{3}{2}\left(u_{\text{wait}} + 2\pi\right)\delta\alpha_0(1)\right) \\ \|\delta\tilde{v}\| \end{bmatrix} \tag{37}$$

In summary, the k^{th} maneuver occurs at target mean argument of latitude u_k and has an RTN $\Delta v_k = \beta_k \Delta\hat{v}$.

We plan new maneuvers whenever the relative distance between the vehicles exceeds the assumed effective laser range of two kilometers. Our targeted rOEs are expressed as

$$\delta\alpha_f = \begin{bmatrix} 0 \\ 0 \\ \Gamma/a_t\cos(\theta_\alpha) \\ \Gamma/a_t\sin(\theta_\alpha) \\ \Gamma/a_t\cos(\theta_\alpha + j\pi) \\ \Gamma/a_t\sin(\theta_\alpha + j\pi) \end{bmatrix} \tag{38}$$

where Γ is a design parameter controlling SE size, $\theta_\alpha \in [0,\, 2\pi)$ controls SE phasing, and $j = 0$ or 1 controls if the δe vector is parallel or anti-parallel to the δi vector. Future work will investigate the implications of targeting a non-zero $\delta\lambda_f$. Our system is agnostic to the θ_α and j values which are actually chosen so we uniformly sample θ_α for both values of j and target the $\delta\alpha_f$ with minimum dV requirements.

RESULTS

To demonstrate the efficacy of our system we simulate a satellite detumbling operation in MATLAB's Simulink environment. Our chaser spacecraft begins in an SE around the target in low Earth orbit. Relevant mission parameters are outlined in Table 1. Key results are summarized in Table 2.

Table 1 The parameters used for validating our detumbling system.

Item	Value
f_{laser}	$4.8978 \times 10^{-5}\,\text{N}$
J_t	$\text{blkdiag}\,(32.6,\ 73.7,\ 79.7)\text{kg}\,\text{m}^2$
m_t	$150\,\text{kg}$
w_0	$1\,\text{deg/s}$
a_t	$6978\,\text{km}$
e_t	10^{-5}
$\begin{bmatrix} l_x & l_y & l_z \end{bmatrix}$	$\begin{bmatrix} 1.0 & 1.3 & 1.0 \end{bmatrix}\text{m}$
Γ	3.58×10^{-5}

Table 2 The key results from our detumbling system validation.

Item	Value
Total dV Requirement	$7.5\,\text{m/s}$
Number of Maneuvers	14
Time to Detumble	$288.6\,\text{hours}$

Figure 7 shows the target's angular momentum during the simulation. The target's angular momentum is monotonically decreasing. Sections in which angular momentum remains constant correspond to periods in which SE restoration maneuvers are being performed.

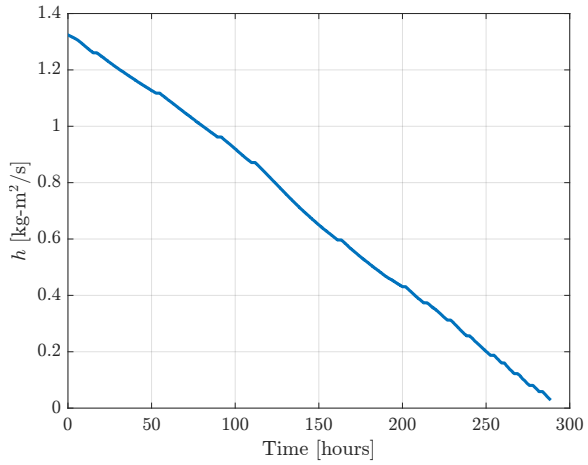

Figure 7 The target's angular momentum during the simulated detumbling operation.

Figure 8 shows the dV requirements for each maneuver sequence. Fourteen sequences are re-

quired over the twelve day detumble operation. The average and maximum dV required for each sequence is $0.53\,\mathrm{m/s}$ and $0.72\,\mathrm{m/s}$, respectively. The sequences appear to increase in frequency as the target's angular momentum decreases. Future work is required to understand this behavior but we hypothesize that the lower target body rate leads to longer periods of laser force which is roughly aligned along one direction. This leads to faster SE degradation.

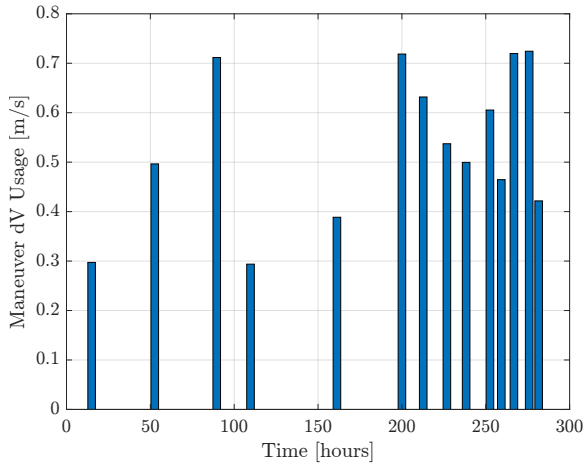

Figure 8 The dV requirements for each three maneuver sequence to restore the SE.

Figure 9 shows our chaser's angular rates. Since the laser is aligned with the body z-axis, almost all rotation is in the body x and y axes. The maximum observed body rates never exceed $0.2\,\mathrm{deg/s}$. A future mission design could use this fact to relax pointing requirements for rotations along the laser axis.

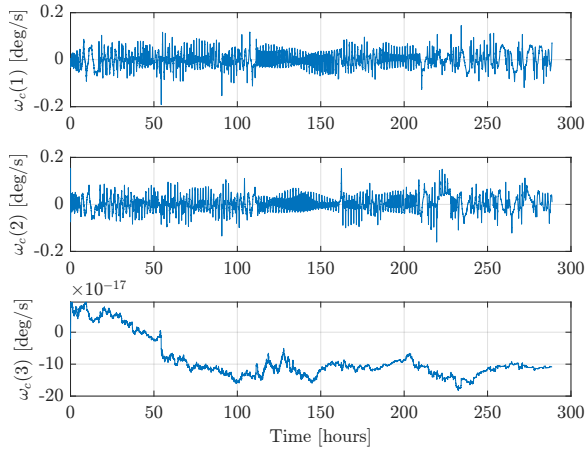

Figure 9 The chaser's angular rate with respect to the inertial frame expressed in the chaser's body frame.

Figure 10 shows the relative separation between the two vehicles. The closest approach between the two vehicles is $54\,\mathrm{m}$. This value occurs during an SE restoration sequence and could be lower than many mission designers would find acceptable. Future work will investigate how the relative motion controller can be tuned to avoid producing maneuver sequences with such close approaches.

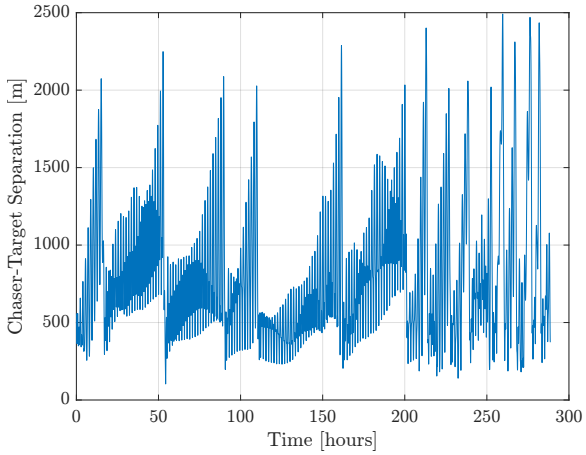

Figure 10 The relative distance between the two vehicles during the detumble simulation.

Laser Force Study

An important mission design consideration is the effective laser force applied to the target. More forceful lasers will provide more torque and result in faster detumble times. However, they also create larger relative accelerations between the two vehicles. As the target tumbles and the chaser moves around the SE, the inertial force applied to the target by very weak lasers will virtually average to zero. This has the effect of preserving our SE. We hypothesize that when the laser is forceful the SE degrades before a full orbit is made and so the SE is no longer centered upon the target. This leads to further SE degradation as the inertial force applied no longer roughly averages to zero. The net effect of this phenomenon is that more forceful lasers can require larger dV budgets to maintain formation flight.

To demonstrate this behavior we perform Monte Carlo simulations with 100 runs at each of nine of laser force levels. The relative motion parameters and target parameters are outlined in Table 3. In each run the target begins with the same magnitude of angular momentum h_0 but the angular momentum's direction is sampled randomly from the unit sphere.

Table 3 The parameters used for the laser force study.

Item	Value
$\log_{10}(f_{\text{laser}}/0.72)$	$[-5, -4.8333, \ldots, -3.666]$ $\log_{10}(\text{N}/0.72)$
J_t	$\text{blkdiag}\,(32.6,\, 73.7,\, 79.7)\text{kg}\,\text{m}^2$
m_t	$150\,\text{kg}$
h_0	$0.43\,\text{kg}\,\text{m}^2/\text{s}$
a_t	$6978\,\text{km}$
e_t	10^{-5}
$\begin{bmatrix} l_x & l_y & l_z \end{bmatrix}$	$\begin{bmatrix} 1.0 & 1.3 & 1.0 \end{bmatrix}\text{m}$
Γ	3.58×10^{-5}

Figure 11 shows box and whisker plots for laser force against chaser dV requirements. dV is relatively constant for laser forces at or below $0.03\,\mathrm{mN}$. Above this level, dV requirements increase dramatically. At the highest tested laser force of $0.16\,\mathrm{mN}$ dV requirements have increase by almost an order of magnitude. The standard deviation of dV has also increased significantly, making it harder to forecast how much fuel will be required for a particular detumbling operation. We hypothesize that for these mission parameters $0.03\,\mathrm{mN}$ is a threshold beyond which the laser causes significant SE degradation over the course of one orbit. Future work is needed to investigate this phenomenon.

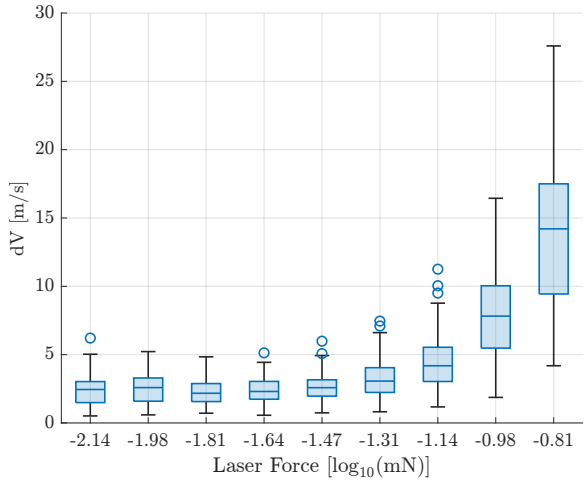

Figure 11 A box and whisker plot for chaser dV requirements across a range of laser forces. A 100 run Monte Carlo is performed at each laser force magnitude. Each blue box corresponds to dV median, upper, and lower quartiles. The black whiskers show the range of values which are not outliers. Any outliers are shown with blue circular marks.

Figure 12 shows box and whisker plots for laser force against time required to detumble the target. Intuitively, more forceful lasers detumble their targets faster. However, returns are diminishing as laser force increases. This is likely due to the increased fraction of mission time spent restoring the SE as laser force grows.

CONCLUSION

We have developed a guidance and control scheme which advances the development of autonomous laser-based detumbling technologies. We've implemented a method for relative motion control during the detumbling process; a problem which has yet to be addressed in the literature. We've also revealed some nonintuitive relationships between laser force and detumbling performance. Intuition might suggest that a more forceful laser would decrease detumble time and therefore mission duration. This would have the effect of reducing mission dV requirements for formation flight maintenance. On the contrary, our results suggest increased laser force appears to dramatically increase dV requirements and provides diminishing returns on reducing detumble time. We hypothesize that weak lasers require less dV as the force imparted upon their target virtually averages to zero over the course of one orbit. This may only be true for naive implementations. Its possible that algorithmic changes to how laser thrust is applied could reduce or eliminate this effect.

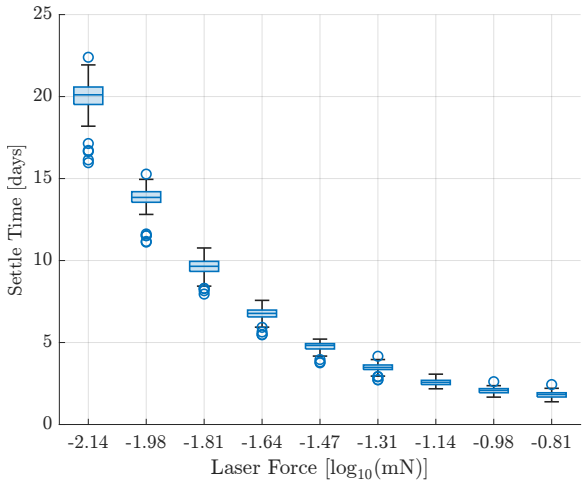

Figure 12 A box and whisker plot for detumble time requirements across a range of laser forces. A 100 run Monte Carlo is performed at each laser force magnitude. Each blue box corresponds to settle time median, upper, and lower quartiles. The black whiskers show the range of values which are not outliers. Any outliers are shown with blue circular marks.

Several avenues for future work have been identified. Primarily, the relationship between laser force and mission performance should be understood on a deeper level. We view these studies as critical for designing a future laser-based detumbling mission. A variety of areas for additional guidance, navigation, and control algorithm development and validation have also been identified. These include increasing chaser attitude control realism, developing a relative navigation scheme, and modifying the guidance law to target a range of safety ellipses instead of one specific set of relative orbital elements.

ACKNOWLEDGMENT

We'd wish to extend our thanks to the Flight Dynamics team and Mission Design Center at NASA Ames Research Center. Their assistance has been invaluable in producing this work.

REFERENCES

[1] "Space Debris by the Numbers," `https://www.esa.int/Space_Safety/Space_Debris/Space_debris_by_the_numbers`. Accessed: 2023-12-20.

[2] H. G. Lewis, "Understanding long-term orbital debris population dynamics," *Journal of Space Safety Engineering*, Vol. 7, No. 3, 2020, pp. 164–170.

[3] D. J. Kessler and B. G. Cour-Palais, "Collision frequency of artificial satellites: The creation of a debris belt," *Journal of Geophysical Research: Space Physics*, Vol. 83, No. A6, 1978, pp. 2637–2646.

[4] R. Hoyt, "Terminator tape: A cost-effective de-orbit module for end-of-life disposal of LEO satellites," *AIAA Space 2009 Conference & Exposition*, 2009, p. 6733.

[5] C. Lücking, C. Colombo, and C. R. McInnes, "Solar radiation pressure-augmented deorbiting: passive end-of-life disposal from high-altitude orbits," *Journal of Spacecraft and Rockets*, Vol. 50, No. 6, 2013, pp. 1256–1267.

[6] Inter-Agency Space Debris Coordination Committee, "IADC Space Debris Mitigation Guidelines," `https://orbitaldebris.jsc.nasa.gov/library/iadc-space-debris-guidelines-revision-2.pdf`, March 2020.

[7] M. A. Foster, "Practical System to Remove Lethal Untracked Orbital Debris," *Journal of Aerospace Information Systems*, Vol. 19, No. 10, 2022, pp. 661–667.

[8] S. Missonnier, L. Lequette, S. Rommelaere, and C. Bonnal, "The space blower concept, a solution for just-in-time collision avoidance," *Proc. 8th European Conference on Space Debris (virtual)*, 2021.
[9] J. W. Campbell, "Project ORION: orbital debris removal using ground-based sensors and lasers," tech. rep., 1996.
[10] C. R. Phipps, "L'ADROIT - A spaceborne ultraviolet laser system for space debris clearing," *Acta Astronautica*, Vol. 104, No. 1, 2014, pp. 243–255.
[11] T. Fukushima, D. Hirata, K. Adachi, Y. Itaya, J. Yamada, K. Tsuno, T. Ogawa, N. Saito, M. Sakashita, S. Wada, *et al.*, "End-of-life deorbit service with a pulsed laser onboard a small satellite," *Proceedings of the 8th European Conference on Space Debris*, 2021.
[12] J. B. Bacon, "Minimum dV for Targeted Spacecraft Disposal," *European Conference on Space Debris*, No. JSC-CN-39184-1, 2017.
[13] T. Wang, "Analysis of Debris from the Collision of the Cosmos 2251 and the Iridium 33 Satellites," *Science & Global Security*, Vol. 18, No. 2, 2010, pp. 87–118.
[14] K. Albee, C. Oestreich, C. Specht, A. Terán Espinoza, J. Todd, I. Hokaj, R. Lampariello, and R. Linares, "A robust observation, planning, and control pipeline for autonomous rendezvous with tumbling targets," *Frontiers in Robotics and AI*, Vol. 8, 2021, p. 641338.
[15] G. S. Aglietti, B. Taylor, S. Fellowes, T. Salmon, I. Retat, A. Hall, T. Chabot, A. Pisseloup, C. Cox, A. Mafficini, *et al.*, "The active space debris removal mission RemoveDebris. Part 2: In orbit operations," *Acta Astronautica*, Vol. 168, 2020, pp. 310–322.
[16] K. Tsuno, S. Wada, T. Ogawa, T. Ebisuzaki, T. Fukushima, D. Hirata, J. Yamada, and Y. Itaya, "Impulse measurement of laser induced ablation in a vacuum," *Optics Express*, Vol. 28, No. 18, 2020, pp. 25723–25729.
[17] J. Michael, K. Chudej, M. Gerdts, and J. Pannek, "Optimal rendezvous path planning to an uncontrolled tumbling target," *IFAC Proceedings Volumes*, Vol. 46, No. 19, 2013, pp. 347–352.
[18] M. M. d. Almeida, R. Zanetti, D. Mortari, and M. Akella, "Real-time angular velocity estimation of non-cooperative space objects using camera measurements," *AAS/AIAA Astrodynamics Specialist Conference*, Vol. 8, 2018.
[19] H. Krag, S. Setty, A. Di Mira, I. Zayer, and T. Flohrer, "Ground-based laser for tracking and remediation–an architectural view," *69th International Astronautical Congress (IAC)*, 2018, pp. IAC–18.
[20] M. Vetrisano, N. Thiry, and M. Vasile, "Detumbling large space debris via laser ablation," *2015 IEEE Aerospace Conference*, IEEE, 2015, pp. 1–10.
[21] D. Sakai, Y. Yoshimura, T. Hanada, Y. Itaya, and T. Fukushima, "Contactless attitude control of an uncooperative satellite by laser ablation," *Acta Astronautica*, Vol. 196, 2022, pp. 275–281.
[22] H. Schaub and D. Stevenson, "Prospects of relative attitude control using coulomb actuation," *The Journal of the Astronautical Sciences*, Vol. 60, 2013, pp. 258–277.
[23] M. Vasile, A. Gibbings, I. Watson, and J.-M. Hopkins, "Improved laser ablation model for asteroid deflection," *Acta Astronautica*, Vol. 103, 2014, pp. 382–394.
[24] S. D'Amico, *Autonomous formation flying in low earth orbit*. PhD thesis, TU Delft, 2010.
[25] S. Shuster, D. Geller, and M. Harris, "Analytic maneuver sequence for safety ellipse reconfigurations using relative orbital elements," *Journal of Guidance, Control, and Dynamics*, Vol. 44, No. 9, 2021, pp. 1593–1606.